Title

P4 Activation by Lanthanum and Lutetium Naphthalene Complexes Supported by a Ferrocene Diamide Ligand

Journal

European Journal of Inorganic Chemistry, 2013(22-23)

ISSN

1434-1948

Authors

Huang, Wenliang
Diaconescu, Paula L

Publication Date

2013-08-06

DOI

10.1002/ejic.201300225

Peer reviewed

DOI: 10.1002/ejic.201

P_4 Activation by Lanthanum and Lutetium Naphthalene Complexes Supported by a Ferrocene Diamide Ligand

Wenliang Huang and Paula L. Diaconescu*

Keywords: P_4 activation / lanthanum and lutetium naphthalene complexes / ferrocene diamide ligand / Zintl-type polyphosphide

Two rare-earth metal (La and Lu) naphthalene complexes supported by a ferrocene diamide ligand activate P_4 under ambient conditions to form M_3P_7 species exclusively. The resulting complexes feature the Zintl type polyphosphide P_7^{3-} unit stabilized by three lanthanide ions supported by the ferrocene diamide ligand. Complexes were characterized by X-ray crystallography, multinuclear NMR spectroscopy, and elemental analysis.

Introduction

The Haber-Bosch process, which converts N_2 from air and H_2 from steam reforming to ammonia, consumes 1-2% of the world's annual energy supply, 3-5% of the world's natural gas production, in order to provide ammonia to the fertilizer industry. Like nitrogen, phosphorus is essential to life and widely used in fertilization. Unlike N_2, white phosphorus, P_4, is the common source of phosphorus in industry and is unstable. It self-ignites in air and converts to the more stable allotrope, red phosphorus, under light or heat. The high reactivity of P_4 is likely due to its weak P-P bond and geometric constraints of the tetrahedron structure. Though easily activated, the activation of P_4 is not easily controlled.[5-7]

P_4 activation by main group and transition metals has been of long-standing interest.[5-7] Alkali metals and late transition metals compose the majority of examples of direct P_4 activation.[5, 6] On the contrary, early transition metal mediated P_4 activation is much less investigated and rare-earth examples are rare.[7-13] Roesky et al. reported the formation of $(Cp^*_2Sm)_4P_8$ from slow vapour transfer of P_4 into a toluene solution of Cp^*_2Sm.[12] Our group recently reported a direct P_4 activation by well defined scandium and yttrium naphthalene or anthracene complexes under ambient conditions.[14] $[(NN^{fc})Sc]_4P_8$ (**Sc_4P_8**) and $[(NN^{fc})Sc]_3P_7$ (**Sc_3P_7**) formed in the scandium case, while $[(NN^{fc})Y(THF)]_3P_7$ (**Y_3P_7**) formed exclusively in the case of yttrium (NN^{fc} = 1,1'-fc(NSi^tBuMe_2)$_2$, fc = ferrocenylene). Herein we report the expansion of this chemistry to two other rare-earth metals, lanthanum and lutetium, that resulted in the isolation and characterization of $[(NN^{fc})La(THF)]_3[(NN^{fc})La(OEt_2)]_2P_7$ (**La_3P_7**) and $[(NN^{fc})Lu(THF)]_3P_7$ (**Lu_3P_7**). The synthesis and characterization of the metal naphthalene complexes $[(NN^{fc})La(THF)]_2(\mu\text{-}C_{10}H_8)$ (**La_2-naph**) and $[(NN^{fc})Lu(THF)]_2(\mu\text{-}C_{10}H_8)$ (**Lu_2-naph**) are also included.

Results and Discussion

Synthesis and structural characterization. We previously reported the synthesis of $[(NN^{fc})Sc]_2(\mu\text{-}C_{10}H_8)$ (**Sc_2-naph**)[15] and $[(NN^{fc})Y(THF)]_2(\mu\text{-}C_{10}H_8)$ (**Y_2-naph**)[14] from the reaction of $(NN^{fc})ScI(THF)_2$ or $(NN^{fc})YI(THF)_2$ with KC_8 and naphthalene. **La_2-naph** and **Lu_2-naph** were prepared by a similar protocol in moderate yield (Eq 1). Compounds **La_2-naph** and **Lu_2-naph** complete the series of diamagnetic lanthanide naphthalene complexes supported by NN^{fc} and allow us to compare their properties. For example, **Sc_2-naph** is a black solid, which is barely soluble in hexanes but soluble in aromatic solvents such as benzene and toluene. However, **Y_2-naph** is a dark-red solid, which is barely soluble in hexanes, aromatic solvents, or even diethyl ether and is only soluble in polar solvents such as THF. Lutetium, like yttrium, binds a molecule of THF and **Lu_2-naph** has similar physical properties to **Y_2-naph**: both are dark-red solids and show the same solubility in polar and non-polar solvents. However, lanthanum, with the largest ionic radius of all lanthanides, leads to **La_2-naph**, which has properties similar to **Sc_2-naph**: it is a black solid soluble in aromatic solvents and even slightly soluble in hexanes. The four examples indicate that it is difficult to predict the properties of rare-earth metal complexes based on their ionic radii as is commonly the practice.

Compounds **La_2-naph** and **Lu_2-naph** were characterized by ^1H and ^{13}C NMR spectroscopy and elemental analysis. While the proton chemical shifts of **Lu_2-naph** were close to the corresponding proton chemical shifts of **Y_2-naph** and **Sc_2-naph**, the proton chemical shifts of the naphthalene fragment in **La_2-**

Department of Chemistry and Biochemistry, University of California, Los Angeles, 607 Charles E. Young Drive East, Los Angeles, CA 90095, U.S.A.
Fax: 1 (310) 206-4038
E-mail: pld@chem.ucla.edu
Homepage: http://copper.chem.ucla.edu/pldgroup/index.htm
Supporting information for this article is available on the WWW under http://www.eurjic.org/ or from the author.

naph were significantly upfield compared to the other three metal naphthalene complexes. For **Sc_2-naph**, **Y_2-naph**, and **Lu_2-naph**, the naphthalene fragments show two sets of multiplets in the ^{1}H NMR spectrum: one at around 5 ppm and the other at 4 ppm. For **La_2-naph**, the corresponding proton chemical shifts were at 4.3 and 2.7 ppm, each shifted upfield by about 1 ppm. However, the ^{13}C chemical shifts for **La_2-naph** were similar to the other metal naphthalene complexes. The reason for the unexpected proton upfield shifting for **La_2-naph** is not clear to us now, especially since the ^{13}C chemical shifts were in the normal range.

The molecular structure of **La_2-naph** (Figure 1) was determined by X-ray crystallography. **La_2-naph** crystallized in the space group *P*-1, while **Y_2-naph** crystallized in $P2_1/n$. The C-C distances within the naphthalene fragment were closer in value to each other than in the case of **Y_2-naph**, ranging from 1.374 to 1.451 Å in **La_2-naph** compared to 1.376 to 1.470 Å in **Y_2-naph**.[14] The two lanthanum fragments are η^4-coordinated to opposite sides of the naphthalene ligand. The distances between lanthanum and the four coordinating carbon atoms were similar, ranging from 2.827to 2.891 Å. Noteworthy, the La-Fe distance is 3.266 Å, which is 0.12 Å shorter than the sum of the metal covalent radii. On the contrary, the corresponding Y-Fe distance in **Y_2-naph** was 3.20 Å, which is close to the sum of metal covalent radii (3.22 Å). Interestingly, the THF free **Sc_2-naph** had a Sc-Fe distance of 2.83 Å, which is about 0.19 Å shorter than the sum of the metal covalent radii.[16] We previously proposed that the electron-rich iron in the ferrocene-based ligand could serve as a Lewis base to a highly Lewis acidic rare-earth metal centre.[15, 17-21] This Lewis acid-base interaction is weak and may be disrupted by strong Lewis bases such as THF, as was the case in **Y_2-naph**, where the extra THF molecule cancelled the weak M-Fe interaction and resulted in a long Y-Fe distance. However, in the case of **La_2-naph**, the La-Fe interaction is maintained even with one extra THF molecule coordinated to lanthanum.

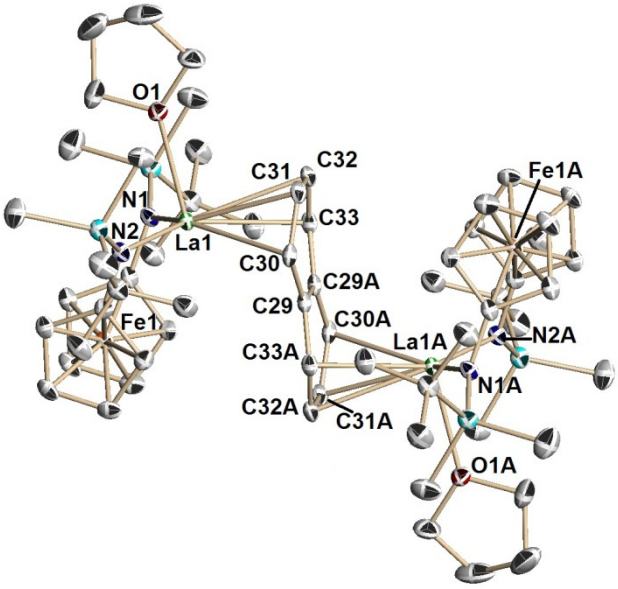

Figure 1. Molecular structure of **La_2-naph** with thermal ellipsoids drawn at the 50% probability level. Only one of the two crystallographically independent molecules is shown here. Hydrogen atoms were omitted for clarity. Lanthanum in green, nitrogen in blue, oxygen in red, silicon in light blue, and carbon in grey. Selected distances [Å] and angles [°]:La1-N1 2.382(2), La1-N2 2.3672(2), La1-O1 2.5342(2), La1-Fe1 3.2659(4), La1-C30 2.891(2), La1-C31 2.841(2), La1-C32 2.827(2), La1-C33 2.865(2), C29-C29A 1.451(5), C29-C30 1.418(3), C30-C31 1.433(4), C31-C32 1.374(4), C32-C33 1.437(4), N1-La-N2 120.28(7), C29A-C29-C30 118.36(28), C29-C30-C31 121.00(22), C30-C31-C32 119.45(24), C31-C32-C33 119.76(23), C32-C33-C29A 120.55(22).

With **La_2-naph** and **Lu_2-naph** in hand, we tested their reactivity toward P_4. Regardless of the stoichiometry of P_4 vs. **M_2-naph**, **La_3P_7** and **Lu_3P_7** were formed exclusively. This behaviour was analogous to that of **Y_2-naph** but different from that of **Sc_2-naph**, which led to two different products, $[(NN^{fc})Sc]_4P_8$ (**Sc_4P_8**) and $[(NN^{fc})Sc]_3P_7$ (**Sc_3P_7**).[14] The exclusive formation of **M_3P_7** in the case of lanthanum and lutetium was expected since **La_2-naph** and **Lu_2-naph** are structurally similar to **Y_2-naph** but different from **Sc_2-naph** because of the extra THF molecule coordinated to scandium. With the exact stoichiometry (Eq 2), the reaction went to complete conversion and naphthalene was the only by-product. ^{31}P NMR spectra of the crude reaction mixture showed peaks only for **M_3P_7**. Crystalline **La_3P_7** and **Lu_3P_7** were isolated in good yield after crystallization from various organic solvents. It was found that **La_3P_7** was more soluble than **Lu_3P_7** in common organic solvents: **La_3P_7** was soluble in hexanes and in aromatic solvents, while **Lu_3P_7** was almost insoluble in hexanes and only slightly soluble in aromatic solvents. While the solubility of **Lu_3P_7** was similar to that of previously reported **Y_3P_7**, the solubility of **La_3P_7** was different but similar to that of the THF free compound **Sc_3P_7**. The unexpected solubility properties of **M_3P_7** (M = Sc, Y, La, Lu) echo the different solubilities of **M_2-naph** described above.

The molecular structures of **La_3P_7** (Figure 2) and **Lu_3P_7** (Figure 3) were determined by single-crystal X-ray diffraction. While **Lu_3P_7** is isostructural to **Y_3P_7** and shows each lutetium with one coordinating THF molecule, **La_3P_7** crystallized in the *P*-1 space group and two out of the three lanthanum atoms coordinate a diethyl ether ligand instead of THF. Different batches of **La_3P_7** showed different ratios between THF and diethyl ether as coordinating solvent molecules. Similar to **La_3P_7**, some batches of **La_2-naph** also had diethyl ether replacing THF based on ^{1}H NMR spectroscopy. We attribute this lack of selectivity between THF and diethyl ether to the weaker Lewis acidity of La(III) when compared to that of Y(III) and Lu(III).[22]

Both **La_3P_7** and **Lu_3P_7** structures feature a central Zintl-type polyphosphide P_7^{3-} anion surrounded by three $(NN^{fc})M(solv)$ fragments. Except for **Sc_3P_7**, which does not coordinate any THF, all the other **M_3P_7** adopt the same coordination environment. The small ionic size of scandium may explain this difference. The lack of THF coordination in **Sc_3P_7** is compensated by a close contact between scandium and the ferrocene backbone, as shown by the extremely short Sc-Fe distance of 2.80 Å, about 0.22 Å shorter than the sum of the covalent radii of scandium and iron.[14] Despite this difference in coordination environment, P-P distances (Table 1) show a clear trend: the larger the rare-earth metal ionic radius, the shorter the P_{edge}-P_{bottom} distance, which is accompanied by a slight lengthening of the other two types of P-P bonds. In alkali earth metal stabilized P_7^{3-} compounds, the three distinguishable P-P bonds also have different distances, with the shortest being P_{edge}-P_{bottom} and the longest the P_{bottom}-P_{bottom} distance within the bottom

triangle.[23] For instance, in Sr_3P_{14}, P_{apex}-P_{edge}, P_{edge}-P_{bottom}, and P_{bottom}-P_{bottom} are 2.21, 2.17, and 2.25 Å, respectively.[24]

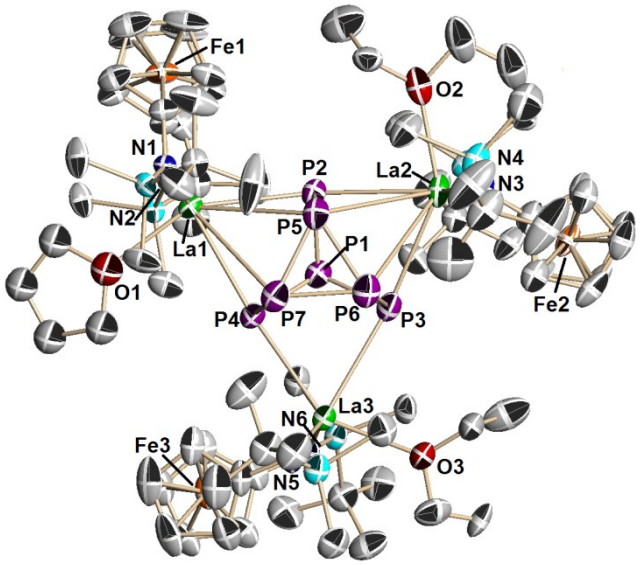

Figure 2. Molecular structure of $\mathbf{La_3P_7}$ with thermal ellipsoids drawn at the 50% probability level. Hydrogen atoms were omitted for clarity. Lanthanum in green, phosphorus in purple, nitrogen in blue, oxygen in red, silicon in light blue, and carbon in grey. Selected distances [Å] and angles [°]: La1-N1 2.355(4), La1-N2 2.333(4), La2-N3 2.354(5), La2-N4 2.334(4), La3-N5 2.322(4), La3-N6 2.324(5), La1-O1 2.558(6), La2-O2 2.620(5), La3-O3 2.594(4), La1-Fe1 3.368(1), La2-Fe2 3.386(1), La3-Fe3 3.427(1), La1-P2 3.111(2), La1-P4 3.108(2), La2-P2 3.113(2), La2-P3 3.127(2), La3-P3 3.179(2), La3-P4 3.079(2), P1-P2 2.192(2), P1-P3 2.184(2), P1-P4 2.197(2), P2-P5 2.155(2), P3-P6 2.167(3), P4-P7 2.162(3), P5-P6 2.265(3), P6-P7 2.241(3), P7-P5 2.267(3), N1-La-N2 128.00(14), N3-La2-N4 126.99(15), N5-La3-N6 125.00(17), P4-La1-P2 65.90(4), P2-La2-P3 65.15(4), P3-La3-P4 64.84(4), P2-P1-P3 100.30(9), P3-P1-P4 100.02(9), P4-P1-P2 100.85(9), P1-P2-P5 99.98(9), P2-P5-P6 105.60(9), P5-P6-P7 60.49(8), P6-P7-P5 60.29(8), P7-P5-P6 59.22(8).

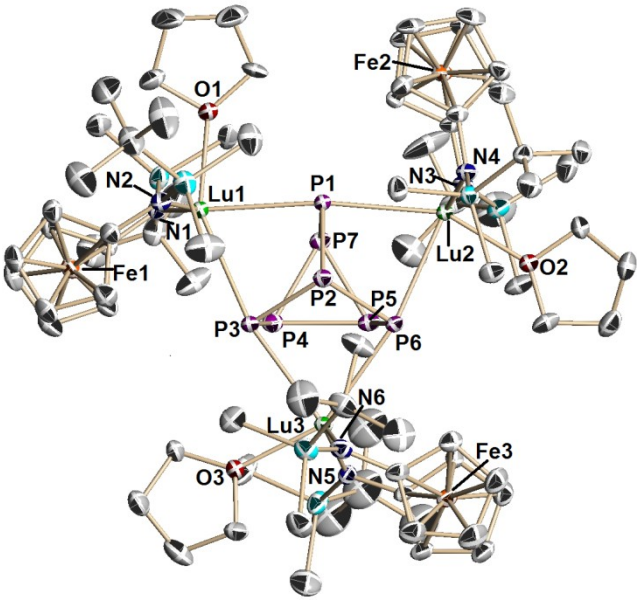

Figure 3. Molecular structure of $\mathbf{Lu_3P_7}$ with thermal ellipsoids drawn at the 50% probability level. Hydrogen atoms were omitted for clarity. Lutetium in green, phosphorus in purple, nitrogen in blue, oxygen in red, silicon in light blue, and carbon in grey. Selected distances [Å] and angles [°]: Lu1-N1 2.184(5), Lu1-N2 2.178(5), Lu2-N3 2.187(5), Lu2-N4 2.170(5), Lu3-N5 2.197(5), Lu3-N6 2.165(5), Lu1-O1 2.298(4), Lu2-O2 2.290(4), Lu3-O3 2.316(4), Lu1-Fe1 3.320(1), Lu2-Fe2 3.265(1), Lu3-Fe3 3.372(1), Lu1-P1 2.862(2), Lu1-P3 2.947(2), Lu2-P1 2.865(2), Lu2-P6 2.897(2), Lu3-P6 2.876(2), Lu3-P3 2.910(2), P1-P2 2.178(2), P2-P3 2.183(2), P2-P6 2.188(2), P3-P4 2.180(3), P6-P5 2.180(2), P1-P7 2.183(2), P4-P5 2.246(2), P5-P7 2.224(2), P7-P4 2.228(2), N1-Lu-N2 127.43(19), N3-Lu2-N4 129.08(19), N5-Lu3-N6 125.10(20), P1-Lu1-P3 69.95(4), P1-Lu2-P6 70.37(4), P6-Lu3-P3 71.39(4), P1-P2-P3 99.56(8), P3-P2-P6 101.13(9), P1-P2-P6 99.02(8), P2-P3-P4 100.56(9), P3-P4-P5 105.34(9), P4-P5-P7 59.79(7), P5-P7-P4 60.60(7), P7-P4-P5 59.61(7).

Table 1. P-P distances of $\mathbf{M_3P_7}$ (unit: Å, error in brackets, all are averaged values).

$\mathbf{M_3P_7}$	P_{apex}-P_{edge}	P_{edge}-P_{bottom}	P_{bottom}-P_{bottom}
$\mathbf{Sc_3P_7}$[a]	2.201(2)	2.197(2)	2.229(2)
$\mathbf{Lu_3P_7}$	2.183(2)	2.181(2)	2.233(2)
$\mathbf{Y_3P_7}$	2.188(2)	2.176(3)	2.238(2)
$\mathbf{La_3P_7}$	2.191(2)	2.161(2)	2.258(2)

[a] Unlike the other $\mathbf{M_3P_7}$, $\mathbf{Sc_3P_7}$ has no THF molecule coordinating to scandium.

In the case of lanthanum, the difference between the P-P distances is comparable to the case of alkali earth P_7^{3-} binary complexes, while for $\mathbf{Sc_3P_7}$, the difference between P-P distances is minimized and actually close to that observed for silyl substituted P_7R_3 organic compounds. For instance, in $P_7(SiMe_3)_3$, P_{apex}-P_{edge}, P_{edge}-P_{bottom}, and P_{bottom}-P_{bottom} distances are 2.180(4), 2.192(4), and 2.214(4) Å.[25] The trend observed by us shows that $\mathbf{M_3P_7}$ (M = Y, La, Lu) compare well to ionic compounds, while $\mathbf{Sc_3P_7}$ is akin to covalent, organic compounds.

Variable temperature NMR spectroscopic studies. P_7^{3-} is the major product of P_4 activation by strong reductants or nucleophiles as well as the "dead-end" of other polyphosphide species decompositions.[6, 23] Intense experimental and theoretical studies have been performed on its alkali and alkali earth metal complexes. For example, Li_3P_7 was studied by variable temperature and 2D ^{31}P NMR spectroscopy,[26-28] and it was found that the ^{31}P NMR spectrum of Li_3P_7 in THF-d_8 is temperature dependent: at low temperature (-60 °C), three distinguishable signals were observed for the three different types of phosphorus atoms in P_7^{3-}; however, upon warming, coalescence took place and, eventually, at high temperature (50 °C) only one peak was observed. This phenomenon was attributed to a fluxional behaviour of P_7^{3-}.[23] The free P_7^{3-} anion can tautomerize to essentially the same tautomer (there are 1680 of them)[28] by simultaneously breaking one P_{bottom}-P_{bottom} bond and forming a new P-P bond between two P_{edge} atoms right next to the two P_{bottom} atoms of the P-P bond that breaks. This tautomerization mechanism, which is analogous to bullvalene tautomerization,[29] was calculated to have a low energy barrier[30] and was further supported by a topology study.[31] Apparently, this tautomerization only takes place in highly ionic compounds like Li_3P_7 and Cs_3P_7;[32] no tautomerization was observed for silyl substituted P_7R_3 compounds.[23] Since the bonding character of rare-earth metals is in between ionic and covalent, and because of our observations of different P-P distances between the four solid state molecular structures, we became interested in studying the solution behaviour of $\mathbf{M_3P_7}$ (M = Sc, Y, La, and Lu).

The ^{31}P NMR spectra of $\mathbf{Sc_3P_7}$, $\mathbf{Y_3P_7}$, and $\mathbf{Lu_3P_7}$, at 25 °C in benzene-d_6 or toluene-d_8, were similar and showed three well resolved peaks that integrated to a 3:1:3 ratio, indicating that the tautomerization of the P_7^{3-} anion was frozen. However, the ^{31}P NMR spectrum (25 °C, benzene-d_6) of $\mathbf{La_3P_7}$ showed only one, broad signal centred at -75 ppm, similarly to Li_3P_7 in THF-d_8.

Therefore, ^{31}P NMR spectra (Figure 4) were collected from -75 °C to 107 °C (**La_3P_7** was stable throughout the variable temperature measurement and even at 85 °C for at least 24 h without any noticeable decomposition).

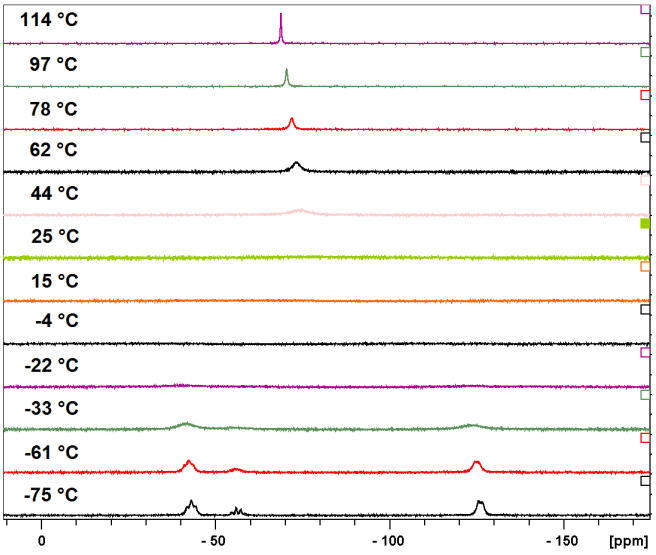

Figure 4. Overlay of ^{31}P NMR spectra (toluene-d_8) of **La_3P_7** at different temperatures. Chemical shifts were referenced to an external standard (85% H_3PO_4) at 25 °C.

The variable temperature ^{31}P NMR spectra clearly showed the fluxional behaviour of P_7^{3-} in **La_3P_7** and a coalescence temperature comparable to that of Li_3P_7. However, surprisingly, this behaviour took place in non-polar solvents (benzene or toluene) for **La_3P_7**, while for Li_3P_7 it was only observed in polar and strongly coordinating solvents such as THF, DME (1,2-dimethoxethane), and TMEDA (tetramethylethylenediamine); without a strongly coordinating solvent, Li_3P_7 decomposes. This difference suggests two possibilities that account for the fluxional behaviour: (1) **La_3P_7** can dissociate to separate ion pairs in non-polar solvents, a behavior that would mimic that of Li_3P_7, and (2) the (NN^{fc})La(THF) fragment can migrate rather easily from one phosphorous atom to another, allowing the valence tautomerization to occur. In the first case, a cationic (NN^{fc})La(THF) species would have to be generated in a non-polar solvent. Although the ferrocene backbone of the NN^{fc} diamide ligand can provide some electronic stabilization and steric shielding, a coordination number of three (two nitrogen and one ferrocene donors) for lanthanum is not reasonable especially in non-polar and weakly coordinating aromatic solvents for **La_3P_7**. Therefore, we dismissed the idea of a separate ion pair in solution. The second possible mechanism for P_7^{3-} tautomerization in **La_3P_7** requires the simultaneous breaking and formation of four La-P bonds (Figure 5). The tautomerization involves one of the five-member rings of P_7^{3-}: a P_{bottom}-P_{bottom} bond breaks while a P_{edge}-P_{edge} bond forms; at the same time, the lanthanum fragment coordinated to that face migrates from two P_{edge} atoms to two P_{bottom} atoms. The other two lanthanum centres only break and form one La-P bond each. Such a process, together with the necessary breaking and formation of P-P bonds, is made possible by the coordination of lanthanum to two neighbouring P_{edge} atoms and two neighbouring P_{bottom} atoms. To support this hypothesis, the average La-P_{edge} distance is 3.10 Å, while the average La-P_{bottom} distance is 3.54 Å. The 0.44 Å difference is smaller than the corresponding distance difference in the other **M_3P_7** (M = Sc: 0.67 Å, Lu: 0.57 Å, Y: 0.53 Å). If it is assumed that the metal-P distances vary linearly with the strength of the metal-P interaction, then it will be easier to form new metal-P bonds for **La_3P_7** than for **Y_3P_7** > **Lu_3P_7** > **Sc_3P_7**. Consequently, we found that the tautomerization also took place in **Y_3P_7** but at a high temperature (coalescence temperature higher than 75 °C). Unfortunately, the low solubility of **Y_3P_7** in aromatic solvents and the high coalescence temperature prevented a detailed variable temperature ^{31}P NMR spectroscopy study for this complex.

Figure 5. Proposed mechanism for valence tautomerization of P_7^{3-} in **La_3P_7** (NN^{fc} ligand and THF molecule were omitted for clarity). The red solid line represents the La-P bond to break. The red dashed line represents the La-P bond to form. The blue solid line represents the P-P bond to break. The blue dashed line represents the P-P bond to form. The black solid line represents the La-P and P-P bonds not affected by this particular tautomerization process.

Conclusions

In summary, we successfully synthesized and characterized the inverse sandwich naphthalene complexes **La_2-naph** and **Lu_2-naph** and utilized them in direct P_4 activation. **La_3P_7** and **Lu_3P_7** were formed exclusively in those reactions. In the two series, **M_2-naph** and **M_3P_7**, **La_2-naph** and **La_3P_7** showed counterintuitive physical properties compared to the other three metal (scandium, yttrium, lutetium) complexes. However, structural data for **M_3P_7** complexes confirm the general trend predicted by the ionic size of rare-earth metals. The tautomerization of the P_7^{3-} anion in **La_3P_7** took place at a similar temperature as in the ionic Li_3P_7 compound, but in non-polar and non-coordinating aromatic solvents. Instead of a separated ion pair mechanism, a lanthanum assisted mechanism was proposed for the valence tautomerization of P_7^{3-} in **La_3P_7**. The ability of rare-earth metals to effect P_4 activation in a controllable fashion as well as their capacity to support the resulting polyphosphide was demonstrated by the exclusive formation of the robust **M_3P_7** family. The Lewis basic ferrocene backbone likely plays an important role to stabilize **M_2-naph** and **M_3P_7** complexes.

Experimental Section

Experimental Details

General considerations. All experiments were performed under a dry nitrogen atmosphere using standard Schlenk techniques or an MBraun inert-gas glove box unless otherwise specified. Solvents, toluene, hexanes, diethyl ether (Et_2O), and tetrahydrofuran (THF) were purified using a two-column solid-state purification system by the method of Grubbs[33] and transferred to the glove box without exposure to air. *n*-Pentane was distilled over calcium hydride under a dinitrogen atmosphere. Methanol was distilled over calcium oxide under a dinitrogen atmosphere. All solvents were stored on activated molecular sieves and/or sodium for at least a day prior to use. NMR solvents, benzene-d_6 (C_6D_6) and toluene-d_8 (C_7D_8), were obtained from Cambridge Isotope Laboratories, degassed or brought

directly into a glove box in a sealed ampoule, and stored over activated molecular sieves for one week prior to use. Naphthalene was bought from Sigma-Aldrich and used as received. P_4 was purified as following: the solid was dissolved in toluene and the resulting solution was passed through neutral alumina and Celite and concentrated under reduced pressure. Colorless or white crystals of P_4 were obtained at -35 °C and stored in a -35 °C freezer prior to use. (NN^{fc})LaI(THF)[34] and (NN^{fc})LuI(THF)$_2$[35] were prepared following literature protocols. Nuclear magnetic resonance (NMR) spectra were recorded on Bruker AV300, Bruker DRX500, Bruker AV500 (work supported by the NSF grants CHE-1048804), or Bruker AV600 spectrometers at 25 °C in C_6D_6 or C_7D_8 unless otherwise specified. Chemical shifts are reported with respect to internal solvent (C_6D_6 at 7.16 ppm or C_7D_8 at 2.09 ppm). CHN analyses were performed in house on a CE-440 Elemental Analyzer manufactured by Exeter Analytical, INC.

Synthesis of La$_2$-naph. (NN^{fc})LaI(THF) (0.5326 g, 0.682 mmol) and naphthalene (0.0416 g, 0.325 mmol) were weighed in a scintillation vial. THF (10 mL) was added to make a yellow solution, which was cooled down to -78 °C with a dry ice / acetone bath. KC_8 (0.106 g, 0.784 mmol) was added to the solution. The reaction mixture was allowed to warm up to 25 °C and stirred for 3 h. The resulting dark red solution was filtered through Celite and dried under reduced pressure. The remaining red solid was dispersed in Et_2O and stored in a -35 °C freezer for 5 days. A blackcrystalline solid was collected on a medium frit after filtration. Yield: 0.289 g, 59.0%. ^{1}H NMR (500 MHz, C_6D_6, 25 °C) δ, ppm: 4.28 and 2.73 (br s, 4H each, C*H* on naphthalene fragement), 4.20 and 3.85 (br s, 8H each, C*H* on Cp rings), 4.09 (br s, 2H, CH_2O on THF), 3.61 (br s, 8H, CH_2O on Et_2O), 1.52 (br s, 2H, CH_2CH$_2$O on THF), 1.26 (m, 12H, CH_3CH$_2$O on Et_2O), 1.01 (s, 36H, (CH_3)$_3$C), and 0.30 (s, 24H, SiCH_3). ^{13}C NMR (126 MHz, C_6D_6, 25 °C) δ, ppm: 156.8, 122.0, 99.5, and 71.0 (*C* or *C*H on naphthalene fragment), 109.4 (CN on Cp rings), broad peaks around 66.8 (*C*H on Cp rings), 27.7 ((CH_3)$_3$C), 20.7 ((CH$_3$)$_3$*C*), and -2.4 (Si*C*H$_3$). An analytical pure sample was obtained by recrystallization from a concentrated hexanes solution in a -35 °C freezer for two days. Anal. (%): Calcd. for $C_{62}H_{100}N_4O_2Fe_2La_2Si_4$, Mw = 1435.354: C, 51.88; H, 7.02; N, 3.90. Found: C, 51.28; H, 7.05; N, 3.46.

Synthesis of Lu$_2$-naph. (NN^{fc})LuI(THF)$_2$ (0.2005 g, 0.226 mmol) and naphthalene (0.0156 g, 0.122 mmol) were weighed in a scintillation vial. THF (6 mL) was added to make a yellow solution which was cooled down to -78 °C with a dry ice / acetone bath. KC_8 (0.451 g, 0.334 mmol) was added to the solution. The reaction mixture was allowed to warm up to 25 °C and stirred for 1 h. The resulting dark red solution was filtered through Celite and dried under reduced pressure. The remaining red solid was dispersed in Et_2O and stored in a -35 °C freezer for 2 days. A red solid was collected on a medium frit after filtration. Yield: 0.0866 g, 51.1%. ^{1}H NMR (500 MHz, C_7D_8, 25 °C) δ, ppm: 5.17 and 4.23 (br s, 4H each, C*H* on naphthalene fragment), 3.96 and 3.87 (br s, 8H each, C*H* on Cp rings), broad peaks around 3.90 (br, 8H, CH_2O on THF), 1.42 (br s, 2H, CH_2CH$_2$O on THF), 1.07 (s, 36H, (CH_3)$_3$C), and 0.26 and 0.15 (s, 12H each, SiCH_3). ^{13}C NMR (126 MHz, C_7D_8, 25 °C) δ, ppm: 154.9, 117.8, and 95.2 (*C* or *C*H on naphthalene fragment), broad peaks around 68.8 (*C*H on Cp rings), 65.9 (*C*H$_2$O on THF), 28.1 ((*C*H$_3$)$_3$C), 25.7 (*C*H$_2$CH$_2$O on THF), and -1.0 and -2.8 (Si*C*H$_3$). Some peaks were missing due to low solubility of **Lu$_2$-naph** or may be masked by deuterated solvent peaks. Anal. (%): Calcd. for $C_{62}H_{100}N_4O_2Fe_2Lu_2Si_4$, Mw = 1507.476: C, 49.39; H, 6.69; N, 3.72. Found: C, 44.78; H, 6.04; N, 3.57. Although multiple samples were submitted for analysis all results were significantly low in carbon. It is possible that fine powders of **Lu$_2$-naph** are extremely air and moisture sensitive and decompose upon handling.

Synthesis of La$_3$P$_7$. To a solution of **La$_2$-naph** (0.1584 g, 0.110 mmol) in THF (6 mL), P_4 (0.0160 g, 0.129 mmol) was added. The color of the solution changed gradually from dark red to orange in 5 min. The reaction mixture was allowed to stir at 25 °C for 1 h. The volatiles were removed under reduced pressure. The resulting yellow-orange solid was extracted in hexanes. After storing in a -35 °C freezer for 6 days, yellow crystals formed and were isolated by decanting the mother liquor and washing with cold *n*-pentane. Yield: 0.0677 g, 42.3%. The formula of single crystals was found to be [(NN^{fc})La(THF)]$_3$[(NN^{fc})La(OEt$_2$)]$_2$P$_7$. The 2:1 ratio of Et_2O:THF of that batch was confirmed by integration of the corresponding peaks in the ^{1}H NMR spectrum. However, a ^{1}H NMR spectrum of another batch, prepared independently, showed exclusively THF as the coordinating solvent molecule. ^{1}H NMR (500 MHz, C_7D_8, 25 °C) δ, ppm: broad peaks centered at 4.11, 3.81, and 3.28 (br, 24H total, C*H* on Cp rings), 3.97 (br s, 6H, CH_2O on THF), 3.56 (br s, 6H, CH_2O on Et_2O), 1.55 (br s, 6H, CH_2CH$_2$O on THF), 1.14 (br s, 9H, CH_3CH$_2$O on Et_2O), 1.10 (s, 54H, (CH_3)$_3$C), and 0.44 (br s, 36H, SiCH_3). ^{13}C NMR (126 MHz, C_7D_8, 25 °C) δ, ppm: 104.9 (*C*N on Cp rings), broad peaks centered at 69.2, 68.2, and 65.0 (*C*H on Cp rings), 28.0 ((CH_3)$_3$C), 25.3 ((CH$_3$)$_3$*C*), and -1.7 (Si*C*H$_3$). Anal. (%): Calcd. for $C_{78}H_{142}N_6O_3Fe_3La_3P_7Si_6$, Mw = 2181.620: C, 42.94; H, 6.56; N, 3.85. Found: C, 43.30; H, 6.75; N, 3.51.

Synthesis of Lu$_3$P$_7$. To a solution of **Lu$_2$-naph** (0.200 g, 0.133 mmol) in THF (12 mL), P_4 (0.0227 g, 0.183 mmol) was added. The color changed gradually from dark red to orange in 10 min. The reaction mixture was allowed to stir at 25 °C for 1 h. The volatiles were removed under reduced pressure. The resulted yellow-orange solid was dissolved in toluene (4 mL) and layered with *n*-pentane (2 mL). After storing in a -35 °C freezer for 2 days, yellow crystals formed and were isolated by decanting the mother liquor and washing with cold *n*-pentane. Yield: 0.109 g, 53.9%. ^{1}H NMR (500 MHz, C_7D_8, 25 °C) δ, ppm: 4.13, 4.07, 3.89, and 3.49 (s, 4H each, C*H* on Cp rings), 4.03 (br s, 12H, CH_2O on THF), 1.53 (br s, 12H, CH_2CH$_2$O on THF), 1.12 (s, 54H, (CH_3)$_3$C), and 0.56 and 0.25 (s, 12H each, SiCH_3). ^{13}C NMR (126 MHz, C_7D_8, 25 °C) δ, ppm: 103.8 (*C*N on Cp rings), 71.0, 67.6, and 65.3 (*C*H on Cp rings), 28.4 ((*C*H$_3$)$_3$C), 25.5 ((CH$_3$)$_3$*C*), and -0.4 and -0.5 (Si*C*H$_3$). Anal. (%): Calcd. for $C_{78}H_{138}N_6O_3Fe_3Lu_3P_7Si_6$ with one molecule of *n*-pentane (C_5H_{12}), Mw = 2357.922: C, 42.28; H, 6.41; N, 3.56. Found: C, 41.93; H, 6.40; N, 3.52.

Supporting Information (see footnote on the first page of this article): Experimental details, NMR spectra, and X-ray data.

Acknowledgments

This work was supported by UCLA, Sloan Foundation, and NSF CAREER. The authors thank the Kaner group (UCLA) for generous gifts of KC_8 and P_4.

[1] V. Smil, *Enriching the Earth: Fritz Haber, Carl Bosch and the Transformation of World Food Production*, The MIT Press, Cambridge, **2001**.

[2] E. H. Oelkers, E. Valsami-Jones, *Elements* **2008**, *4*, 83.

[3] G. M. Filippelli, *Elements* **2008**, *4*, 89.

[4] J. Emsley, *The 13th Element: The Sordid Tale of Murder, Fire, and Phosphorus*, John Wiley & Sons, Inc., New York, **2000**.

[5] M. Caporali, L. Gonsalvi, A. Rossin, M. Peruzzini, *Chem. Rev.* **2010**, *110*, 4178.

[6] M. Scheer, G. Bala´zs, A. Seitz, *Chem. Rev.* **2010**, *110*, 4236.

[7] B. M. Cossairt, N. A. Piro, C. C. Cummins, *Chem. Rev.* **2010**, *110*, 4164.

[8] W. W. Seidel, O. T. Summerscales, B. O. Patrick, M. D. Fryzuk, *Angew. Chem. Int. Ed.* **2009**, *48*, 115.

[9] E. Hey, M. F. Lappert, J. L. Atwood, S. G. Bott, *J. Chem. Soc., Chem. Commun.* **1987**, 597.

[10] P. J. Chirik, J. A. Pool, E. Lobkovsky, *Angew. Chem. Int. Ed.* **2002**, *41*, 3463.

[11] O. J. Scherer, M. Swarowsky, H. Swarowsky, G. Wolmershäuser, *Angew. Chem. Int. Ed.* **1988**, *27*, 694.

[12] S. N. Konchenko, N. A. Pushkarevsky, M. T. Gamer, R. Köppe, H. Schnöckel, P. W. Roesky, *J. Am. Chem. Soc.* **2009**, *131*, 5740.

[13] T. Li, J. Wiecko, N. A. Pushkarevsky, M. T. Gamer, R. Köppe, S. N. Konchenko, M. Scheer, P. W. Roesky, *Angew. Chem. Int. Ed.* **2011**, *50*, 9491.

[14] W. Huang, P. L. Diaconescu, *Chem. Commun.* **2012**, *48*, 2216

[15] W. Huang, S. I. Khan, P. L. Diaconescu, *J. Am. Chem. Soc.* **2011**, *133*, 10410.

[16] B. Cordero, V. Gomez, A. E. Platero-Prats, M. Reves, J. Echeverria, E. Cremades, F. Barragan, S. Alvarez, *Dalton Trans.* **2008**, 2832.

[17] W. Huang, C. T. Carver, P. L. Diaconescu, *Inorg. Chem.* **2011**, *50*, 978.

[18] P. L. Diaconescu, *Comments Inorg. Chem.* **2010**, *31*, 196

[19] P. L. Diaconescu, *Acc. Chem. Res.* **2010**, *43*, 1352.

[20] M. J. Monreal, P. L. Diaconescu, *Organometallics* **2008**, *27*, 1702.

[21] C. T. Carver, M. J. Monreal, P. L. Diaconescu, *Organometallics* **2008**, *27*, 363.

[22] H. Tsuruta, T. Imamoto, K. Yamaguchi, *Chem. Commun.* **1999**, 1703

[23] M. Baudler, K. Glinka, *Chem. Rev.* **1993**, *93*, 1623.

[24] W. Dahlmann, H. G. Schnering, *Naturwissenschaften* **1972**, *59*, 420.

[25] W. Hönle, P. D. H. G. V. Schnering, *Z. Anorg. Allg. Chem* **1978**, *440*, 171.

[26] M. Baudler, T. Pontzen, J. Hahn, H. Temberger, W. Faber, *Z. Naturjorsch.* **1980**, *35b*, 517.

[27] M. Baudler, J. Hahn, *Z. Naturjorsch.* **1990**, *45b*, 1279.

[28] M. Baudler, H. Temberger, W. Faber, J. Hahn, *Z. Naturjorsch.* **1979**, *34b*, 1690.

[29] G. Schröder, J. F. M. Oth, R. Merényi, *Angew. Chem. Int. Ed.* **1965**, *4*, 752.

[30] M. C. Bōhm, R. Gleiter, *Z. Naturjorsch.* **1981**, *36b*, 498.

[31] M. Randic, D. O. Oakland, D. J. Klein, *J. Comput. Chem.* **1986**, *7*, 35.

[32] F. Kraus, J. C. Aschenbrenner, N. Korber, *Angew. Chem. Int. Ed.* **2003**, *42*, 4030.

[33] A. B. Pangborn, M. A. Giardello, R. H. Grubbs, R. K. Rosen, F. J. Timmers, *Organometallics* **1996**, *15*, 1518.

[34] W. Huang, B. M. Upton, S. I. Khan, P. L. Diaconescu, *Organometallics* **2013**, DOI: 10.1021/om3010433.

[35] W. Huang, F. Dulong, T. Wu, S. I. Khan, J. T. Miller, T. Cantat, P. L. Diaconescu, *Nat. Commun.* **2013**, *4*, 1448.

Received:
Published online:

Entry for the Table of Contents

Key Topic

Zintl-type P_7^{3-} complexes were synthesized from direct activation of P_4 by lanthanum and lutetium naphthalene complexes. The P_7^{3-} complexes showed fluxional behaviour dependent on the rare-earth metal.

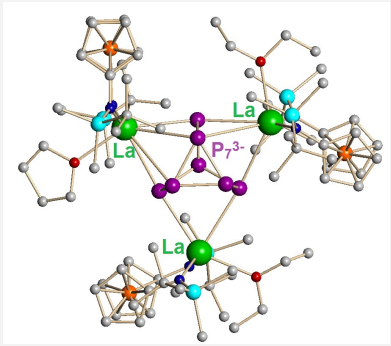

Wenliang Huang and Paula L. Diaconescu* …….Page No. – Page No.

P_4 Activation by Lanthanum and Lutetium Naphthalene Complexes Supported by a Ferrocene Diamide Ligand

Keywords: P_4 activation / naphthalene complexes / ferrocene diamide ligand / Zintl-type polyphosphide